Calsyntenin 1-mediated trafficking of axon guidance receptors regulates the switch in axonal responsiveness at a choice point

Alther, Tobias A ; Domanitskaya, Elena ; Stoeckli, Esther T

The Company of Biologists

RESEARCH ARTICLE

Calsyntenin 1-mediated trafficking of axon guidance receptors regulates the switch in axonal responsiveness at a choice point

Tobias A. Alther, Elena Domanitskaya and Esther T. Stoeckli*

ABSTRACT

Axon guidance at choice points depends on the precise regulation of guidance receptors on the growth cone surface. Upon arrival at the intermediate target or choice point, a switch from attraction to repulsion is required for the axon to move on. Dorsal commissural (dI1) axons crossing the ventral midline of the spinal cord in the floor plate represent a convenient model for the analysis of the molecular mechanism underlying the switch in axonal behavior. We identified in chick a role for calsyntenin 1 in the regulation of vesicular trafficking of guidance receptors in dI1 axons at choice points. In cooperation with RabGDI, calsyntenin 1 shuttles Rab11-positive vesicles containing Robo1 to the growth cone surface in a precisely regulated manner. By contrast, calsyntenin 1-mediated trafficking of frizzled 3, a guidance receptor in the Wnt pathway, is independent of RabGDI. Thus, tightly regulated insertion of guidance receptors, which is required for midline crossing and the subsequent turn into the longitudinal axis, is achieved by specific trafficking.

KEY WORDS: Commissural axon guidance, Frizzled 3, RabGDI, GDI1, Robo1, Wnt signaling, Midline crossing, Chicken

INTRODUCTION

Attractive and repulsive guidance cues cooperate in the navigation of growing axons to their correct targets during development. On their way to the final target, axons may contact one or several intermediate targets. At each one of them, growth cones need to change their responsiveness in order to overcome the attraction derived from the intermediate target and to continue their journey.

The dI1 population of commissural neurons has been widely used to study the molecular mechanisms of axon guidance (Chédotal, 2011; Nawabi and Castellani, 2011). They extend their axons ventrally towards the floor plate, the structure that forms the midline of the neural tube. During this first stage of growth, axons are repelled by BMPs (Augsburger et al., 1999) and Draxin (Islam et al., 2009), chemorepellents derived from the roof plate. At the same time, axons are attracted by the floor plate-derived chemoattractants Netrin (Kennedy et al., 1994) and Shh (Charron et al., 2003). The interaction of axonin 1 (contactin 2) and NgCAM (L1CAM) is responsible for axonal fasciculation along the ventral pathway, whereas the interaction between axonal axonin 1 and floor plate NrCAM is responsible for floor plate entry (Stoeckli and Landmesser, 1995; Stoeckli et al., 1997). RabGDI (GDI1)-dependent insertion of Robo1 into the growth cone membrane triggers sensitivity to the midline-associated repellent Slit1 (Philipp

Institute of Molecular Life Sciences and Neuroscience Center Zurich, University of Zurich, Winterthurerstrasse 190, Zurich CH-8057, Switzerland.

*Author for correspondence (esther.stoeckli@imls.uzh.ch)

et al., 2012). Upon floor plate exit, post-crossing commissural axons turn rostrally guided by two opposing morphogen gradients (Stoeckli, 2006). Wnt gradients in mouse (Lyuksyutova et al., 2003) and in chick (Domanitskaya et al., 2010; Avilés and Stoeckli, 2016) were shown to attract post-crossing axons. At the same time, axons were repelled by a rostral^{low}-caudal^{high} gradient of Shh (Bourikas et al., 2005). Shh shapes the Wnt gradient by inducing the expression of the endogenous Wnt antagonists Sfrp1 and Sfrp2 in a rostral^{low}-caudal^{high} gradient (Domanitskaya et al., 2010). Thus, Shh has multiple roles in commissural axon guidance: it attracts pre-crossing axons to the intermediate target in a Boc- and Smo-dependent manner (Charron et al., 2003; Okada et al., 2006). Then, it affects post-crossing axons both directly and indirectly by shaping the Wnt activity gradient. The direct repulsive effect on post-crossing axons is mediated by Hhip (Bourikas et al., 2005). Recently, we demonstrated that Shh itself regulates the expression of Hhip in a glypican 1-dependent manner (Wilson and Stoeckli, 2013).

The transcriptional regulation of Hhip by its own ligand, Shh, represents one mechanism explaining the switch in axonal responsiveness at the intermediate target. Furthermore, Shh was suggested to induce the responsiveness to semaphorin 3B, a floor plate-derived repellent (Parra and Zou, 2010). Semaphorin 3B binds to a receptor complex consisting of neuropilin 2 and plexin A1. On pre-crossing axons, plexin A1 is destabilized and therefore not expressed on the growth cone surface due to proteolysis by Calpain (Nawabi et al., 2010). Upon axonal arrival at the floor plate, Calpain is inhibited in an NrCAM- (Nawabi et al., 2010) and GFRα1/NCAM-dependent manner (Charoy et al., 2012). This, in turn, results in stabilization and surface expression of plexin A1 and thus responsiveness to the floor plate-derived repellent semaphorin 3B as well as Slit1 (Delloye-Bourgeois et al., 2015).

In the visual system, responsiveness to semaphorin 3A was shown to be regulated at the post-transcriptional level by miR124 (Baudet et al., 2012). Our observation of the regulation of Robo1 surface expression at the post-translational level by RabGDI suggested trafficking as yet another mechanism to switch axonal responsiveness at choice points (Philipp et al., 2012).

RabGDI, which is encoded by a gene linked to human mental retardation (D'Adamo et al., 1998), is an essential component of the vesicle fusion machinery (Seabra et al., 2002; Pfeffer and Aivazian, 2004). RabGDI associates with Rab11-positive vesicles (Philipp et al., 2012). Likewise, an association of Rab11-positive vesicles with calsyntenin 1 was found in kinesin 1-dependent axonal transport (Konecna et al., 2006; Steuble et al., 2010). Calsyntenin 1 is a member of a family of three transmembrane proteins (Vogt et al., 2001; Hintsch et al., 2002) and acts as a linker between vesicular cargo and kinesin 1, the motor for anterograde axonal transport (Konecna et al., 2006). Two binding sites in the cytoplasmic domain of calsyntenin 1 were found to interact with the tetratricopeptides of kinesin light chain 1 (KLC1). Mutations in these domains of

DEVELOPMENT

calsyntenin 1 result in reduced fast anterograde axonal transport (Konecna et al., 2006). In zebrafish, calsyntenin 1-mediated vesicle trafficking is required for branching of peripheral but not central axons of sensory neurons (Ponomareva et al., 2014).

We found calsyntenins to be expressed in a dynamic, partially overlapping pattern in the developing chicken spinal cord. In particular, we found calsyntenin 1 to be expressed in commissural neurons at the time when their axons reach the floor plate and cross the midline. Because calsyntenin 1 was found associated with Rab11-positive vesicles (Steuble et al., 2010, 2012) and because Robo1-positive vesicles requiring RabGDI for membrane insertion of their cargo were also Rab11 positive (Philipp et al., 2012), we analyzed these associations further and found a partial overlap of calsyntenin 1 with Robo1-, Rab11- and RabGDI-positive vesicles both in COS7 cells and in growth cones of commissural axons.

Downregulation of calsyntenin 1 resulted in similar axon guidance defects, as observed after silencing Robo1 or RabGDI. In contrast to Robo1 and RabGDI, loss of calsyntenin 1 had an additional effect on post-crossing commissural axons. Like Shh (Bourikas et al., 2005; Wilson and Stoeckli, 2013), Wnts (Domanitskaya et al., 2010; Avilés and Stoeckli, 2016), SynCAMs (Niederkofler et al., 2010) and semaphorin 6B (Andermatt et al., 2014), calsyntenin 1 was required for the rostral turning of post-crossing commissural axons. Our detailed *in vivo* analyses indicate a regulatory role of calsyntenin 1-mediated trafficking in midline crossing by controlling Robo1 expression and in longitudinal axon guidance by controlling frizzled 3 expression.

RESULTS

Commissural axons lacking calsyntenin 1 stall at the midline and fail to turn into the longitudinal axis

We first detected calsyntenin 1 mRNA in dI1 commissural neurons at HH21 (not shown), and more clearly at HH22, when the first axons have reached the ipsilateral floor plate border in the lumbar spinal cord (Fig. S1). We used *in ovo* RNAi to investigate a potential function of the calsyntenins in commissural axon guidance. To this end, we analyzed the trajectory of dI1 axons after downregulation of calsyntenin 1 in open-book preparations of spinal cords collected from embryos at HH25 (Fig. 1A). In untreated (Fig. 1B) and in control-injected (Fig. 1C) embryos dI1 axons had crossed the midline and turned rostrally along the contralateral floor plate border. After downregulation of calsyntenin 1 in dI1 neurons with a microRNA (miR)-based construct targeting calsyntenin 1 driven by the *Math1* enhancer (miCst1, Fig. 1D) or by electroporation of double-stranded (ds) RNA (dsCst1, Fig. 1E), axon guidance was severely perturbed (Fig. 1F). Axons stalled in the floor plate and failed to turn into the longitudinal axis. On average, only 22.5±5.2% of the injection sites showed normal axonal navigation after injection and electroporation of miCst1. Similarly, after targeting calsyntenin 1 with dsCst1, only 27.7±2.8% of the injection sites showed normal axon guidance. No, or only minor, effects were observed when either calsyntenin 2 or 3 was silenced, as 72.0±4.4% (miCst2) or 56.2±9.3% (dsCst2) and 46.7±4.0% (miCst3) or 63.0± 8.4% (dsCst3) of the injection sites were normal (not shown; Table 1). Calsyntenin 2, which is not expressed in dI1 neurons, served as a negative control, demonstrating the specificity of our approach. Although calsyntenin 3 is expressed in dI1 neurons, its downregulation did not affect commissural axon guidance (Table 1). The efficiency of downregulation was demonstrated by *in situ* hybridization (Fig. S1E,F, Table S1).

Calsyntenin 1 had a direct effect on axonal navigation, as its downregulation did not affect spinal cord patterning. The expression
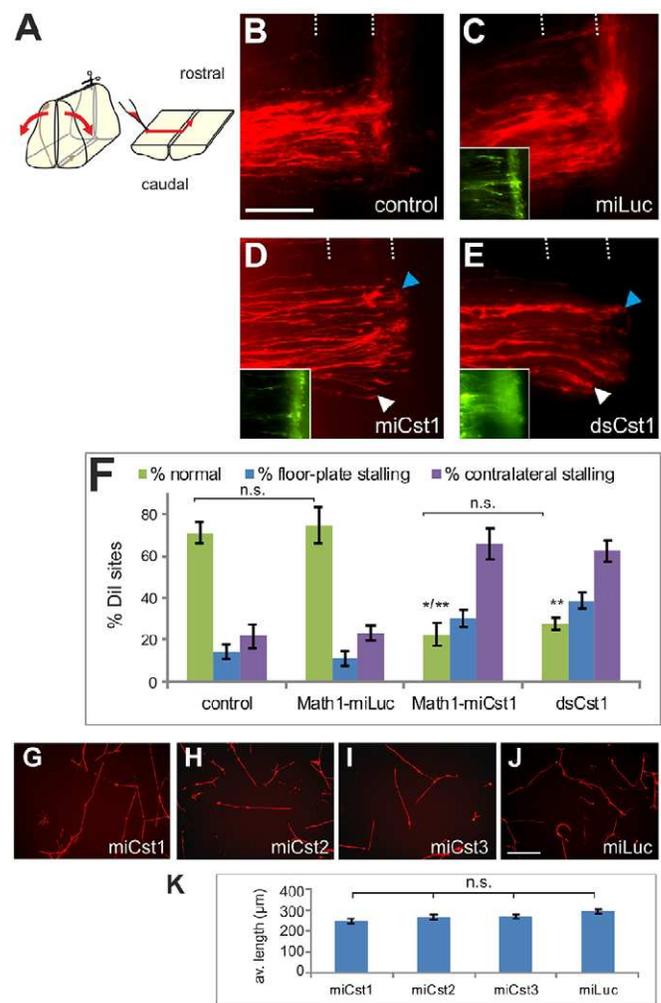
Fig. 1. Silencing calsyntenin 1 perturbs commissural axon navigation. (A) Dorsal (dI1) commissural axons were labeled by DiI injections (red) in open-book preparations of chick spinal cords. (B-F) At HH25, axons in untreated (B) and control-injected (C) embryos had crossed the floor plate and turned rostrally along the longitudinal axis. By contrast, injection and electroporation of a Math1-driven microRNA (miR) construct targeting calsyntenin 1 (miCst1; D) or dsRNA derived from calsyntenin 1 (dsCst1; E) resulted in axons stalling in the floor plate (white arrowhead) or their failure to turn into the longitudinal axis (blue arrowhead). Dotted lines indicate floor plate. Insets (C-E) show GFP expression as injection control. Pathfinding was quantified as detailed in the Materials and Methods (F; see also Table 1). On average, 75.0±8.5% of injection sites had normal axon pathfinding in control embryos injected and electroporated with a miR construct targeting Luciferase (miLuc). This value did not significantly differ from that for untreated embryos (71.1± 5.1%). By contrast, after downregulation of calsyntenin 1 specifically in dI1 neurons with Math1-miCst1, normal axonal navigation was observed on average in only 22.5 ±5.2% of the injection sites. This value was almost identical to that for dsRNA (dsCst1, 27.7±2.8%). (G-K) Calsyntenin 1 affects the guidance, not growth, of commissural axons. Downregulation of calsyntenin 1 (G), calsyntenin 2 (H) or calsyntenin 3 (I) did not affect neurite length of dissociated dorsal root ganglion axons as compared with axons dissected from embryos electroporated with miLuc (J). No significant differences in average neurite lengths between the conditions were found (K). *P<0.05 for Math1-miCst1 compared with untreated control group; **P<0.01 for Math1-miCst1 versus Math1-miLuc control and dsCst1 versus both control groups; n.s., not significant. Values are given ±s.e.m. Scale bars: 100 µm.

of cell type-specific marker proteins did not differ between experimental and untreated control embryos (not shown). Furthermore, the phenotype was not due to a delay in axon

Table 1. Quantification of axon guidance phenotypes

Injected construct(s)	Normal injection sites %	s.e.m.	Floor plate stalling %	s.e.m.	Contralateral stalling %	s.e.m.	Embryos #	Injection sites #
miCst1	22.5	5.2	30.2	4.3	65.9	7.5	11	129
miCst2	72.0	4.4	12.7	3.6	19.5	4.4	11	118
miCst3	46.7	4.0	19.1	4.1	44.8	5.2	11	105
miFzd3	27.7	6.1	6.6	2.3	69.3	6.2	11	137
miRobo1	20.6	3.7	63.5	3.0	32.5	5.3	13	126
miRabGDI	28.4	3.3	63.4	3.5	26.8	3.6	15	183
miCst1 (low)	64.9	5.2	8.5	4.3	28.7	7.5	10	97
miFzd3 (low)	67.0	8.5	10.4	3.9	28.3	8.7	10	106
miRobo1 (low)	67.7	3.5	13.7	3.3	29.4	3.8	10	102
miRabGDI (low)	60.2	5.6	5.4	2.4	25.8	2.9	15	156
miCst1+miFzd3	23.9	5.1	21.1	5.3	70.6	5.5	11	109
miCst1+miRobo1+miRabGDI	35.2	3.1	50.9	2.8	30.8	3.1	12	159
miCst1+miRabGDI	27.3	3.7	49.6	6.2	37.4	4.8	10	139
miCst1+miRobo1 E3	29.3	5.7	30.7	7.0	54.7	6.3	10	75
miCst1+miRobo1 E2	27.8	4.3	55.6	3.3	27.8	3.9	10	126
miRobo1+miFzd3	55.7	3.2	17.1	4.2	36.4	4.0	14	140
miRabGDI+miFzd3	65.9	1.5	11.9	2.7	31.1	1.9	11	135
miCst1 E2	28.8	6.7	37.6	4.7	53.6	6.3	11	125
miRabGDI+RabGDI (rescue)	64.1	6.8	12.4	2.7	27.6	5.1	11	145
miFzd3+EGFP-Fzd3 (rescue)	61.7	3.6	14.2	4.0	34.4	3.4	12	183
miLuc control E3	75.0	8.5	10.9	3.3	23.2	3.5	13	138
miLuc control E2	70.2	3.1	7.6	2.3	25.2	3.8	11	131
Untreated control	71.1	5.1	14.1	3.3	21.5	5.8	15	121
dsRNA-injected embryos (analyzed at HH25/26)								
dsCst1	27.7	2.8	38.6	3.7	62.4	5.4	10	101
dsCst2	56.2	9.3	21.9	6.5	30.5	7.2	11	124
dsCst3	63.0	8.4	15.1	8.7	27.4	6.5	10	103
dsCst1+EGFP-Cst1 (rescue)	62.8	3.4	17.9	4.2	25.2	3.2	11	145
dsCst1+ΔCst1	35.4	2.2	36.7	2.9	48.3	4.5	11	147
EGFP control	77.7	6.1	15.5	2.9	23.4	3.8	14	146
dsRNA-injected embryos (analyzed at HH28)								
dsCst1	32.8	5.5	32.0	6.9	55.5	5.8	12	128
EGFP control	75.0	4.9	9.4	2.7	20.8	4.0	12	96
Untreated control	81.0	3.8	5.4	2.1	13.5	3.6	11	74

The mean percentages (with s.e.m.) of the observed phenotypes per embryo seen for the treatment groups indicated on the left. Note that the two aberrant phenotypes (floor plate stalling and contralateral stalling) are not mutually exclusive and therefore the values do not add up to the difference between percentage normal phenotype and 100%. E2, E3: day of injection and electroporation (see Materials and Methods for details). mi, microRNA construct targeting the respective gene; dsRNA, double-stranded RNA derived from the respective gene; ΔCst1, calsyntenin 1 with mutated kinesin 1 binding sites; 'low' indicates a subthreshold concentration of miR construct that does not induce effective target gene silencing.

outgrowth or a slower growth rate, as axons reached the floor plate at the appropriate stage (Fig. S1G,H) and axons in embryos sacrificed 1 day later still failed to turn into the longitudinal axis (Fig. S1I-L). Similarly, neurite length did not differ between control-treated sensory neurons and neurons lacking calsyntenins grown on laminin (Fig. 1G-K).

Taken together, our in vitro and in vivo experiments demonstrate a role for calsyntenin 1 in commissural axon guidance during floor plate crossing and in the subsequent turning into the longitudinal axis.

Calsyntenin 1 partially overlaps with Robo1, RabGDI and Rab11

The aberrant axon guidance phenotype observed in the absence of calsyntenin 1 strongly resembled the phenotype observed in the absence of RabGDI (Philipp et al., 2012). Because calsyntenin 1 was shown in biochemical studies to be associated with Rab11-positive vesicles (Steuble et al., 2010, 2012) and because our previous in vivo studies indicated that Robo1-containing vesicles regulated by RabGDI were also Rab11 positive (Philipp et al., 2012), we tested for a role of calsyntenin 1 in the regulation of Robo1 surface expression.

We verified partial colocalizations of Robo1, Rab11, RabGDI and calsyntenin 1 in commissural neurons (Fig. 2). Because antibodies for the detection of endogenous proteins are not available, we expressed tagged proteins in commissural neurons in vivo at HH17. After 2 days, we sacrificed the embryos and dissected commissural neuron explants to visualize individual growth cones. We did not include Robo2 in these analyses because the lack of Robo2 was shown to result primarily in ipsilateral turns and, thus, a phenotype different from that obtained after downregulation of calsyntenin 1, Robo1 or RabGDI (Philipp et al., 2012). We also excluded calsyntenin 2 and 3, as their downregulation did not cause any significant changes in commissural axon guidance (Table 1).

We found partial overlap between calsyntenin 1 and Robo1 (Fig. 2A), RabGDI (Fig. 2D) and Rab11 (Fig. 2F). We confirmed our previous observations of a colocalization of Robo1 and Rab11 (Fig. 2B) and RabGDI and Robo1 (Fig. 2C), as well as RabGDI and Rab11 (Fig. 2E) (Philipp et al., 2012). The Pearson's colocalization coefficients of the double-stained axons are given in Fig. 2H. The values from both positive and negative controls (Fig. 2G,H) were significantly different from all other conditions (ANOVA, $P<0.05$). As a positive control, we used an HA-Robo1-myc construct that was
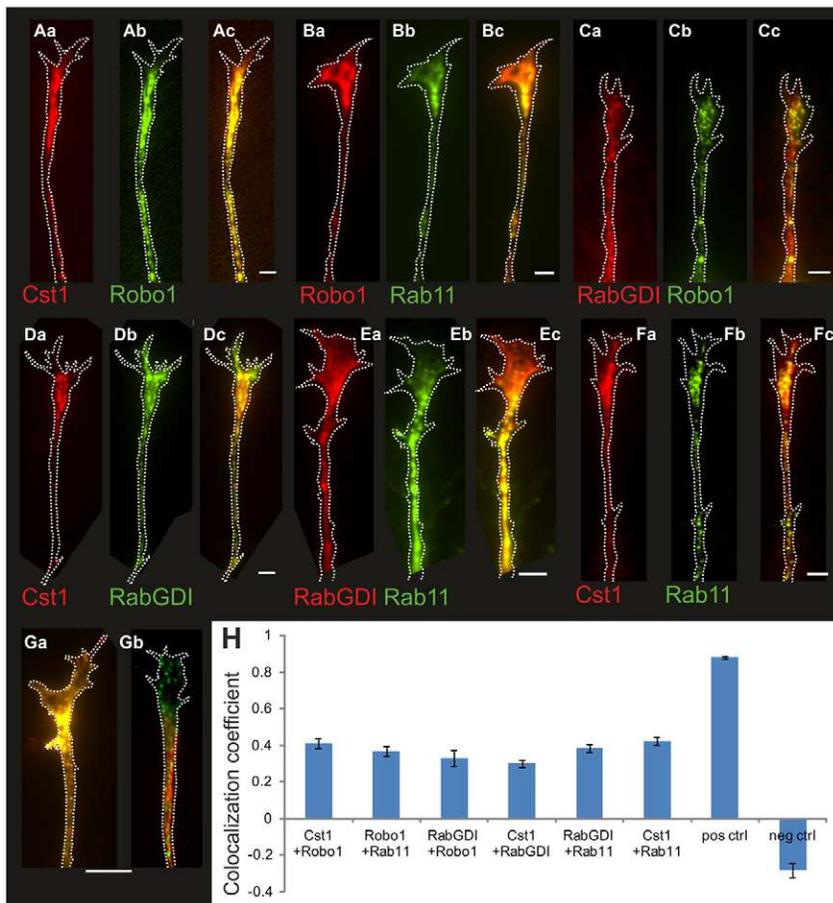
Fig. 2. Calsyntenin 1, RabGDI and Rab11 partially colocalize with Robo1-positive vesicles. Commissural neurons were dissected from HH25 embryos electroporated with combinations of mCherry-calsyntenin 1 and tagged forms of RabGDI, Rab11 or Robo1 (Table S3). After 24-36 h *in vitro*, axons were fixed and stained with anti-tag antibodies. Confocal image analysis followed by deconvolution indicated partial overlap between immunoreactivities for calsyntenin 1 (Cst1) and Robo1 (A), Robo1 and Rab11 (B), RabGDI and Robo1 (C), calsyntenin 1 and RabGDI (D), RabGDI and Rab11 (E), calsyntenin 1 and Rab11 (F). Ac-Fc show merge. Colocalization coefficients (±s.e.m.) are given in H. As a positive control, we stained double-tagged Robo1 with antibodies against both tags (for total overlap, Ga,H), and we stained neurofilament (red) and tubulin (green) as a negative control, showing no overlap (Gb,H). Scale bars: 5 μm.

stained for both tags (HA in green, myc in red). As a negative control, we stained growth cones for tubulin (green) and neurofilament (red). We also used triple staining to confirm partial colocalization of calsyntenin 1, Robo1, RabGDI and Rab11 (Fig. S2).

Taken together, our colocalization studies suggest the existence of calsyntenin 1-positive vesicles containing Robo1 as cargo. In agreement with previous studies, Robo1-containing vesicles are associated with RabGDI and Rab11, suggesting that at least a subpopulation is also positive for calsyntenin 1.

Calsyntenin 1 and RabGDI cooperate in commissural axon guidance at the floor plate

To obtain functional evidence for a potential cooperation between calsyntenin 1 and RabGDI in the regulation of Robo1 surface expression, we electroporated miR-based constructs at subthreshold or 'hypomorphic' doses. If calsyntenin 1 and RabGDI act in the same pathway, then the use of low doses should reproduce the phenotypes observed after efficient downregulation of either RabGDI or Robo1 alone. For a direct comparison, we repeated the silencing of RabGDI and Robo1 obtained previously with dsRNA (Philipp et al., 2012) but using miR constructs (Fig. S3).

As expected, downregulation of Robo1 (Fig. S3A) or RabGDI (Fig. S3B) with 700 ng/μl Math1-driven miR constructs resulted in axonal stalling in the floor plate, as seen previously when we electroporated dsRNA derived from *Robo1* or *RabGDI* (Table 1) (Philipp et al., 2012). When we used only low doses of miRs (300 or 350 ng/μl), downregulation of Robo1 (Fig. S3C), RabGDI

(Fig. S3D) or calsyntenin 1 (Fig. S3E) was less effective and did not result in axonal pathfinding errors (Table 1, Fig. S3F).

However, co-injection of low concentrations of all these miRs together did result in the expected phenotype, i.e. axons stalled in the floor plate and those that did reach the contralateral floor plate border failed to turn rostrally along the longitudinal axis (Fig. 3A,E, Table 1). Similarly, reducing both calsyntenin 1 and RabGDI together by electroporation of low doses was sufficient to induce floor plate stalling (Fig. 3B,E). These results indicate that calsyntenin 1 and RabGDI cooperate in commissural axon guidance.

The combination of low doses of calsyntenin 1 and Robo1 was less efficient in inducing floor plate stalling (at 30.7±7.0% of the injection sites per embryo) but still interfered markedly with correct axon guidance at the floor plate exit site in comparison with control-treated embryos (Fig. 3C,E). At HH18, *Robo1* mRNA is already detected in dI1 neurons (Philipp et al., 2012). Thus, we reasoned that the weaker effect on axonal midline crossing might be due to the presence of Robo1 protein in vesicles already at the time of electroporation at HH18. Thus, we repeated the electroporation of miCst1 together with miRobo1 at HH15. In agreement with our hypothesis, we now found floor plate stalling at 55.6±3.3% of the injection sites (Table 1).

In summary, the *in ovo* perturbation experiments together with our previous findings on the role of RabGDI in Robo1 trafficking (Philipp et al., 2012) suggest a cooperation of calsyntenin 1 and RabGDI in the regulation of Robo1 trafficking to the growth cone surface.
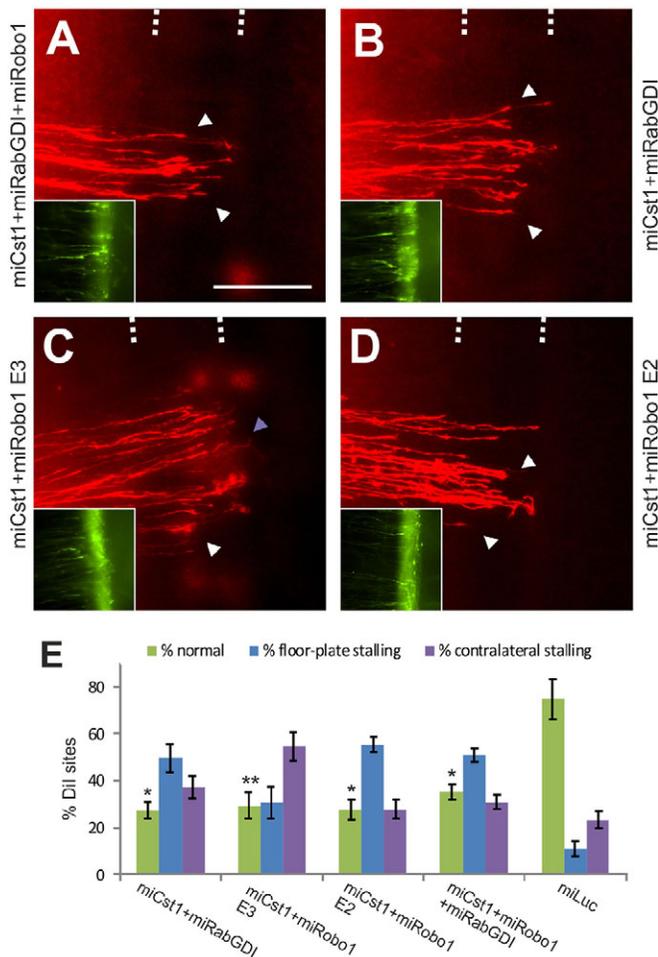
Fig. 3. Calsyntenin 1 cooperates with Robo1 in commissural axon guidance. Co-injection and electroporation of low doses of miCst1, miRabGDI and miRobo1 results in axonal stalling in the floor plate (white arrowheads, A). Similarly, co-electroporation of low doses of only miCst1 and miRabGDI also interfered with axonal pathfinding (B). Co-injection of miCst1 and miRobo1 at E3 did interfere with axon guidance, but resulted in a qualitatively different phenotype, as axons mainly stalled at the contralateral floor plate exit site (purple arrowhead, C). By contrast, electroporation of miCst1 and miRobo1 at E2 reproduced the floor plate stalling phenotypes seen in the absence of both calsyntenin 1 and RabGDI (D). Insets show GFP expression as injection control. These differences are reflected in the quantitative analysis of the experimental groups (E). Note, in addition to the comparison for the normal phenotypes (green bars), all blue bars are significantly different from that for miLuc, except for miCst1+miRobo1 at E3, indicating that floor plate stalling is less affected when miRobo1 is transfected only at E3. Values for miCst1/miRobo1/miRabGDI, miCst1/miRabGDI and miCst1/miRobo1(E2) were virtually identical. *$P<0.05$, **$P<0.01$ in comparison to miLuc. Error bars indicate s.e.m. Scale bar: 100 µm.

Calsyntenin 1 and RabGDI cooperate in Robo1 trafficking

To demonstrate that loss of RabGDI and calsyntenin 1 function indeed affected axon guidance by preventing Robo1 surface expression we assessed the surface levels of double-tagged Robo1 under different conditions (Fig. 4). After downregulation of both calsyntenin 1 and RabGDI, we found significantly less Robo1 on the surface of dI1 growth cones (Fig. 4A,E). As shown previously (Philipp et al., 2012), downregulation of RabGDI alone also interfered with Robo1 surface expression (Fig. 4B,E). The same was true for downregulation of calsyntenin 1 (Fig. 4C,E).

Further evidence for the specificity and the underlying mechanism of Robo1 trafficking was provided by rescue

experiments (Fig. 5). The effect on midline crossing induced by a miR targeting chicken *RabGDI* was rescued by co-electroporation of a plasmid encoding human RABGDI that was not targeted by miRabGDI (Fig. 5A). The effect of loss of calsyntenin 1, induced by dsRNA derived from the 3′ UTR, was reversed by co-electroporation of a plasmid encoding EGFP-tagged calsyntenin 1 that was not targeted (Fig. 5B). However, the effect of calsyntenin 1 silencing could not be rescued by a mutated version of calsyntenin 1 that lacked the binding sites to kinesin 1 (Konecna et al., 2006) and, therefore, was unable to mediate linkage of the vesicle to the transport system (Fig. 5C). Taken together, these results indicate that Robo1 delivery and surface expression on commissural growth cones depend on both RabGDI and calsyntenin 1. Furthermore, the function of calsyntenin 1 depends on its role in vesicle trafficking.

Calsyntenin 1 cooperates with frizzled 3

Comparison of the phenotypes seen after silencing calsyntenin 1 or RabGDI revealed qualitative differences. In the absence of RabGDI most axons failed to reach the contralateral floor plate border. Therefore, the behavior of post-crossing axons was difficult to assess. Silencing calsyntenin 1 also affected midline crossing, but more axons reached the contralateral floor plate border. However, most post-crossing axons failed to turn into the longitudinal axis. Thus, we analyzed the behavior of post-crossing axons in more detail.

In previous studies, we characterized the role of morphogen signaling in post-crossing commissural axon guidance. Both Shh (Bourikas et al., 2005; Wilson and Stoeckli, 2013) and Wnt signaling (Domanitskaya et al., 2010; Avilés and Stoeckli, 2016; see also Lyuksyutova et al., 2003) were shown to be required for the rostral turn of post-crossing commissural axons along the longitudinal axis of the spinal cord. Because pre-crossing axons are not sensitive to the Shh and Wnt gradients, the surface expression of guidance receptors needs to be temporally regulated in a precisely controlled manner. The expression of Hhip, the receptor mediating the repulsive response to Shh, was shown to be regulated at the transcriptional level (Bourikas et al., 2005; Wilson and Stoeckli, 2013). A colocalization of Hhip and calsyntenin 1 was therefore not expected. Indeed, that is what we found, when Hhip and calsyntenin 1 were expressed in COS7 cells (Fig. S4).

By contrast, immunoreactivities of calsyntenin 1 and frizzled 3 (Fzd3), the receptor for Wnts, strongly overlapped in COS7 cells (Fig. 6A) and in commissural axons and growth cones (Fig. 6B). *Fzd3* mRNA was found in dI1 commissural neurons already at HH18 (Fig. 6C). Therefore, regulation of Fzd3 at a post-transcriptional level was required to explain why post-crossing, but not pre-crossing, axons were responsive to Wnt. In agreement with the temporal expression pattern, downregulation of Fzd3 with dsRNA at HH18/19 did not effectively prevent the rostral turn of post-crossing commissural axons, as normal axon pathfinding was seen at 88.7% of all injection sites. By contrast, after silencing Fzd3 at HH14/15, we found robust interference with the rostral turning of post-crossing commissural axons. Normal pathfinding was only seen at 21.8% of the injection sites. These values were similar in embryos electroporated with a miR targeting *Fzd3* (Fig. 6E,H). We found axons that failed to turn rostrally along the contralateral floor plate border at $69.3\pm6.2\%$ (miFzd3) of all injection sites. These results are in agreement with previous studies in the mouse (Lyuksyutova et al., 2003).

To assess whether calsyntenin 1 is required for the regulation of Fzd3 expression, we again used *in ovo* RNAi with hypomorphic concentrations of miRs (Fig. 6F,H). We decreased the amount of
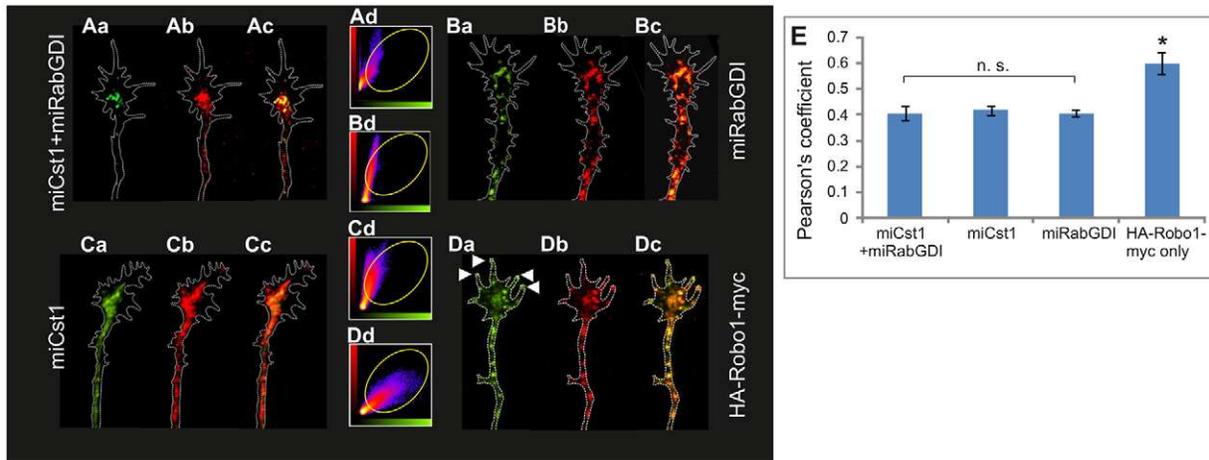
Fig. 4. Trafficking of Robo1 to the growth cone surface depends on both calsyntenin 1 and RabGDI. Surface levels of Robo1 were determined by staining live cells prior to fixation and permeabilization with an antibody against the N-terminal tag (green, Aa-Da). After fixation and permeabilization, staining for the C-terminal tag revealed total levels of Robo1 (red, Ab-Db). Merged images are shown in Ac-Dc. Quantification of colocalized puncta as scatter plots (Ad-Dd) and Pearson's coefficients is shown (E). Robo1 surface levels decreased after perturbation of both calsyntenin 1 and RabGDI together (each miR injected at low dose; A), or each of them individually when injected at high, effective doses (B,C), as compared with the control condition in which the HA-Robo1-myc construct was transfected without miRs (D). ***$P<0.001$ for comparison of Pearson's coefficient calculated for control versus all other conditions. Error bars indicate s.e.m.

miR until the injection of either the miR targeting *Fzd3* (67.0±8.5% of the injection sites with normal axon guidance) or that targeting calsyntenin 1 alone (64.9±5.2% of the injection sites with normal axon guidance) did not significantly interfere with post-crossing commissural axon guidance. However, when we co-injected the low levels of miRs against calsyntenin 1 and *Fzd3* most axons reached the contralateral border of the floor plate but failed to turn rostrally at 70.6±5.5% of the injection sites (Fig. 6G,H, Table 1).

Taken together, these results indicate a cooperation of calsyntenin 1 and Fzd3 in post-crossing commissural axon guidance.

Calsyntenin 1 regulates Fzd3 expression independently of RabGDI

Based on the temporal expression of Fzd3 and the role of calsyntenin 1 in vesicle trafficking, we expected calsyntenin 1 to regulate Fzd3 surface expression. Using a similar approach as that detailed above, we analyzed Fzd3 trafficking to the growth cone surface (Fig. 7). Downregulation of calsyntenin 1 together with RabGDI did reduce Fzd3 on the surface but only to the same extent that was achieved with loss of calsyntenin 1 alone. Silencing RabGDI alone did not change the surface expression of Fzd3 compared with the control (compare Fig. 7B with D, quantified in E).

The absence of an effect of RabGDI on Fzd3 surface expression was corroborated by functional data. When we electroporated low amounts of miR constructs targeting *Fzd3* and *RabGDI*, we did not observe any increase in axon guidance errors compared with control embryos (Fig. 7F,H; 65.9±1.5%). Thus, we concluded that RabGDI is not required for Fzd3 trafficking to the growth cone surface.

Our findings were further supported by the detailed analysis of Robo1 and Fzd3 expression. Although both Robo1-positive and Fzd3-positive vesicles were mostly immunopositive for calsyntenin 1, Robo1 and Fzd3, immunoreactivity barely overlapped (Fig. 8). These findings support our *in vivo* data implicating calsyntenin 1 in both Robo1 and Fzd3 trafficking. However, in contrast to Robo1, Fzd3 trafficking is independent of RabGDI. Most likely, calsyntenin 1 is also required for the trafficking of additional vesicles containing as yet unknown cargoes, as many vesicles that were calsyntenin 1-positive were not associated with either Fzd3 or Robo1.

In summary, our *in vivo* studies demonstrate a crucial role for calsyntenin 1 in the specific trafficking of guidance receptors to the growth cone surface at a choice point. The storage of guidance receptors in Rab11-positive vesicles in growth cones allows for their rapid insertion into the membrane. In turn, the surface expression of novel guidance receptors changes the responsiveness of the growth cone to the intermediate target and, thus, forces the axon to continue with its navigation toward the next intermediate or its final target. Furthermore, the rapid insertion of guidance receptors at a choice point, in this case the floor plate, rather than their accumulation on the surface over time explains why axons acquire responsiveness to the guidance cues for the longitudinal axis only after midline crossing.

DISCUSSION

Midline crossing by dI1 commissural axons represents an easily accessible model with which to study the molecular mechanisms underlying the required switch in axonal responsiveness at a choice point. Pre-crossing axons enter the floor plate due to the predominance of positive signals derived from the interaction of the growth cone with guidance cues expressed by floor plate cells. However, in order to leave the floor plate and move on towards the final target, axons need to overcome this attraction. Therefore, growth cones need to change their surface receptors to recognize previously undetectable repulsive cues associated with the intermediate target. At the floor plate, these negative cues have been identified as Slits (Brose et al., 1999; Yuan et al., 1999) and class 3 semaphorins (Nawabi et al., 2010; Zou et al., 2000). Furthermore, axons need to ignore the guidance cues directing them along the longitudinal axis on the ipsilateral floor plate border but readily detect them upon floor plate exit. Both floor plate crossing and turning into the longitudinal axis therefore depend on the precisely regulated expression of guidance receptors on the growth cone surface.

Responsiveness to semaphorin 3B and Slit was shown to depend on the stabilization of the surface receptor component plexin A1 (Nawabi et al., 2010; Charoy et al., 2012; Delloye-Bourgeois et al., 2015) and to involve Shh-dependent sensitization (Parra and Zou,
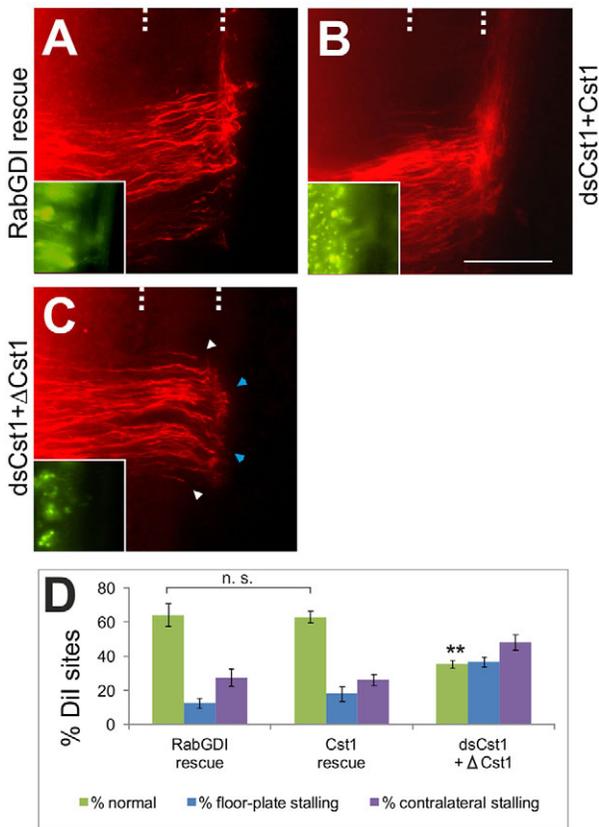
Fig. 5. The transport function of calsyntenin 1 is required for correct axon guidance at the midline. The effects of silencing RabGDI and calsyntenin 1 on axonal pathfinding could be rescued by co-expression of non-targeted ORFs of RabGDI and wild-type calsyntenin 1, respectively. Co-expression of human RABGDI that was not targeted by miRabGDI (which was designed against chicken RabGDI) rescued the axon guidance defects caused by silencing endogenous RabGDI (A,D). Similarly, co-injection of a plasmid encoding EGFP-tagged calsyntenin 1 together with dsRNA derived from the 3′ UTR of chicken calsyntenin 1 prevented the pathfinding errors seen after silencing calsyntenin 1 (B,D). However, a mutated version of calsyntenin 1 that lacked the binding sites for kinesin 1 motors, and was therefore unable to mediate vesicle trafficking, could not rescue the axon guidance defect (C,D, white and blue arrowheads). Insets show EGFP expression as injection control. **$P<0.01$ in comparison to each rescue. Error bars indicate s.e.m. Scale bar: 100 μm.

2010). The sensitivity to Slit1 was triggered by the RabGDI-dependent trafficking of Robo1 to the growth cone surface (Philipp et al., 2012). In mouse, a switch in Robo3 isoform expression was suggested to contribute to the regulation of Robo1-mediated sensitivity to Slit of pre-crossing versus post-crossing commissural axons (Chen et al., 2008). However, these findings have been questioned recently (Zelina et al., 2014).

Similarly, the regulation of axonal responsiveness to guidance cues for the longitudinal axis depends on the precisely controlled surface expression of guidance receptors. An example of regulation at the transcriptional level is provided by our findings that Shh induces the expression of its own receptor Hhip for the guidance of post-crossing axons in a glypican 1-dependent manner (Wilson and Stoeckli, 2013; Bourikas et al., 2005). By contrast, responsiveness of post-crossing axons to Wnts is regulated by trafficking of Fzd3 to the growth cone surface (this study). This trafficking must not be confused with the endocytosis of Fzd3 shown to be part of Wnt signaling in axon guidance (Onishi et al., 2013; Shafer et al., 2011).
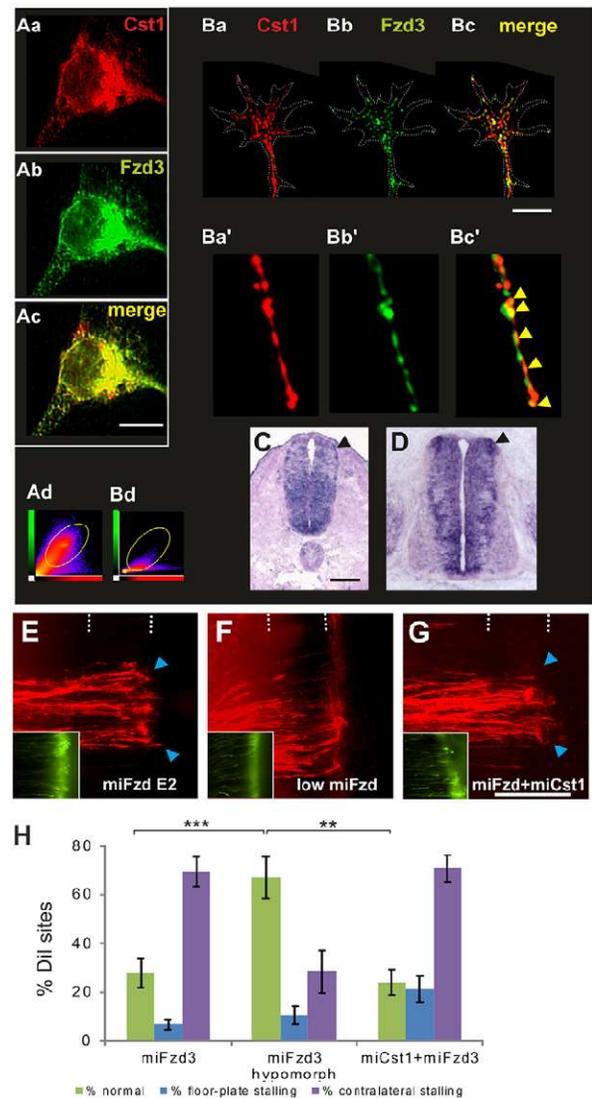
Fig. 6. Calsyntenin 1 is required for frizzled 3 trafficking. Calsyntenin 1 and frizzled 3 (Fzd3) colocalize in COS7 cells (A; Pearson's coefficient 0.75, scatter plot Ad), in growth cones (B; Pearson's coefficient 0.56, scatter plot Bd) and in commissural axons (B′, yellow arrowheads). *Fzd3* mRNA was already detected in dI1 neurons at HH18, that is, when dI1 axons start to extend in the dorsal lumbar spinal cord (C, black arrowhead), and was maintained at HH24, when axons exit the floor plate and turn into the longitudinal axis (D). In line with the temporal expression pattern, downregulation of Fzd3 at E3 did not perturb commissural axon guidance (not shown), whereas electroporation of dsFzd3 (not shown) or miFzd3 at E2 did interfere with commissural axon guidance (E,H; Table 1). Axons failed to turn into the longitudinal axis at the contralateral floor plate border (blue arrowheads). Electroporation of the same miFzd3 at low dose did not significantly interfere with axonal turning (F,H), in contrast to co-electroporation of miFzd3 and miCst1 at E2 (G,H). Insets show GFP expression. (H) Comparison of percentage of DiI injection sites with normal axon guidance. After silencing Fzd3 at E2 with the effective (full) dose of miFzd3, normal axon guidance was observed only at 27.7±6.1% of the injection sites. This was similar to the value obtained after co-downregulation of Fzd3 and calsyntenin 1 (23.9±5.1%). By contrast, after electroporation of the low dose of miFzd3 normal axon guidance was seen at 67.0±8.5% of injection sites. Similarly, when we compared rostral turns at the floor plate exit site, we found significant differences between the effect of low levels of miFzd3 as compared with both miFzd3 at the effective dose and the co-injection and electroporation of both miCst1 and miFzd3. **$P<0.01$, ***$P<0.0001$. Both conditions were significantly different from controls ($P<0.0001$). Error bars indicate s.e.m. Scale bars: 5 μm in A,B; 100 μm in C-G.
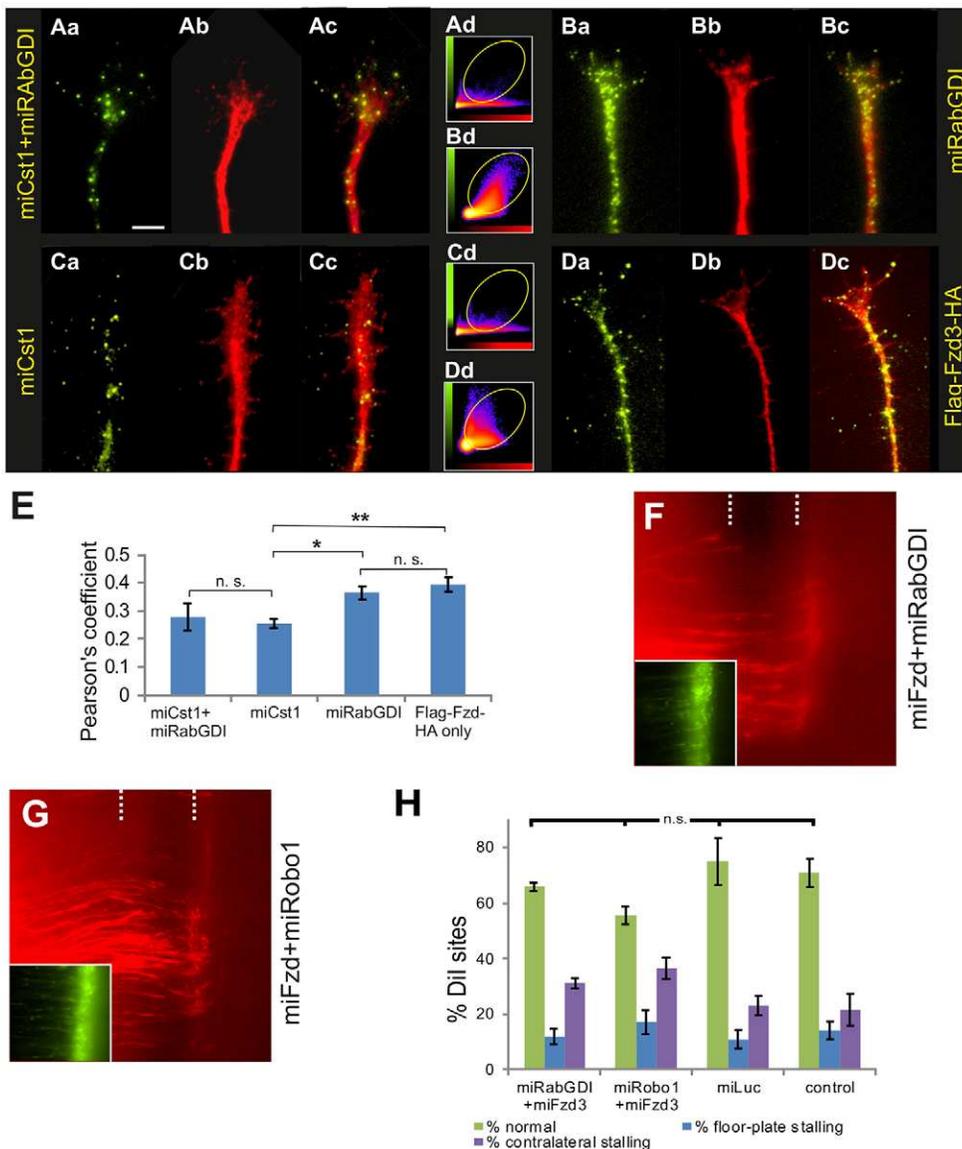
Fig. 7. Fzd3 trafficking to the growth cone surface depends on calsyntenin 1 but is independent of RabGDI. (A-E) Surface Fzd3 was visualized by staining live cells prior to fixation and permeabilization with an antibody against the N-terminal Flag tag (green, Aa-Da). After fixation and permeabilization, staining for the C-terminal HA tag revealed total Fzd3 (red, Ab-Db). Merged images are shown in Ac-Dc. The quantification of co-stained puncta is shown in Ad-Dd and E (Pearson's coefficients). Relative surface levels of Fzd3 decreased after perturbation of both calsyntenin 1 and RabGDI together (each miR injected at low dose; A), but only to the same level as seen after silencing calsyntenin 1 alone (C,E). Silencing RabGDI did not interfere with surface expression of Fzd3 (B). Levels were very similar to the control condition, where Flag-Fzd3-HA was expressed in the absence of miRs (D,E). Silencing calsyntenin 1 effectively reduced the surface levels of Fzd3 (*$P<0.05$ compared with dsRabGDI; **$P<0.01$ compared with Flag-Fzd3-HA). (F-H) In agreement with these observations on Fzd3 trafficking, the co-injection of low doses of miRabGDI and miFzd3 (F,H) or miRobo1 together with miFzd3 (G,H) did not affect axon guidance at the midline. Normal pathfinding was observed at 65.9±1.5% of the injection sites for miRabGDI/miFzd3, and at 55.7±3.2% of the injection sites for miRobo1/miFzd3. These values do not differ from those for control groups (values taken from Fig. 1), where we observed normal pathfinding at 75.0±8.5% for miLuc and 71.1±5.1% for untreated controls. Error bars indicate s.e.m. Scale bar: 5 μm.

In response to Wnt binding, Fzd3 was shown to be internalized in an Arf6-dependent manner for signal transduction. In our study, we describe the molecular basis of trafficking for the initial delivery of Fzd3 to the growth cone surface, explaining why growth cones do not respond to the Wnt gradient along the ipsilateral floor plate border.

Both our previous *in vivo* studies characterizing the role of RabGDI in Robo1 regulation (Philipp et al., 2012) and the studies characterizing the role of calsyntenin 1 in Robo1 and Fzd3 regulation reported here, indicate that RabGDI and calsyntenin 1 are not required for axonal growth but specifically for axon guidance.

Loss-of-function and rescue experiments indicate that the role of calsyntenin 1 in commissural axon guidance depends on its binding to kinesin, the motor for anterograde axonal transport of vesicles. An effect of calsyntenin 1 on the selective transport of vesicle subpopulations containing guidance receptors as cargo is in agreement with our findings that calsyntenin 1-positive puncta colocalized with puncta positive for either Robo1 or Fzd3, both axon guidance receptors whose surface expression needs to be

precisely regulated at the floor plate to prevent premature reactivity to the respective ligands Slits and Wnts. Furthermore, the expression of neither Robo1 nor Fzd3 is regulated at the transcriptional level.

The regulation of vesicle trafficking and thus the specificity of cargo delivery to the growth cone surface in a temporally precisely regulated manner represents a potent molecular mechanism underlying the switch in axonal responsiveness at an intermediate target. Our results indicate that the regulatory mechanisms for the trafficking of Robo1 and Fzd3 differ. Robo1 surface expression depends on both RabGDI and calsyntenin 1 (Fig. 4) (Philipp et al., 2012). By contrast, RabGDI was not required for the regulation of Fzd3 surface expression on post-crossing versus pre-crossing axons (Fig. 7).

Thus, the most parsimonious explanation of these results is the regulation of trafficking of vesicles with specific guidance receptors as cargo. One type of vesicle contains Robo1 receptors. This type of vesicle requires both RabGDI and calsyntenin 1 for fusion with the plasma membrane and insertion of Robo1 into the growth cone membrane. Another type of vesicle that contains Fzd3 as cargo is
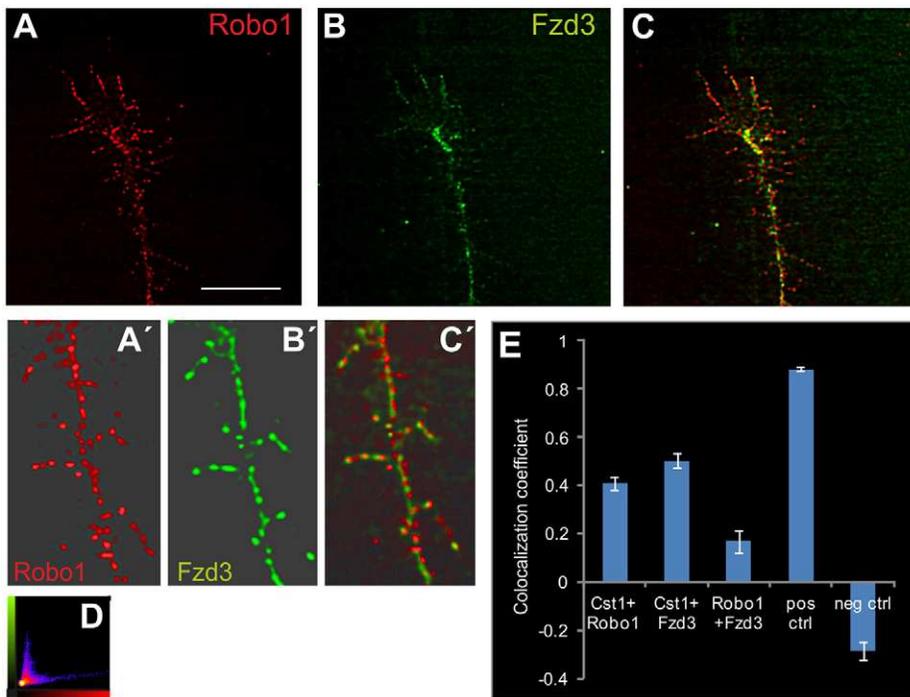
Fig. 8. Robo1 and Fzd3 are trafficked differently to the growth cone surface. Our functional results are consistent with observations that Robo1-positive vesicles (A, red) barely overlap with Fzd3-positive vesicles (B, green); merged image (C). The lack of overlap is evident at higher magnification (A′-C′). A scatter plot (D) also indicates poor overlap between Robo1 and Fzd3. This is reflected by the Pearson's coefficient (E). Values for positive and negative controls are taken from Fig. 2H. Error bars indicate s.e.m. Scale bar: 5 µm.

independent of RabGDI but requires calsyntenin 1 for trafficking to the growth cone membrane. These results are in perfect agreement with a recent study in zebrafish, where loss of calsyntenin 1 was found to affect branching of peripheral but not central sensory axons (Ponomareva et al., 2014). These findings were linked to the observation that calsyntenin 1 was associated with a specific subpopulation of vesicles. The same concept – subpopulations of vesicles with specific cargo – is also found in our study demonstrating a regulatory role of vesicular trafficking of guidance receptors to the growth cone surface to orchestrate the switch in axonal behavior at intermediate targets or choice points.

MATERIALS AND METHODS

In ovo RNAi and open-book preparation

Fertilized chicken eggs obtained from a local hatchery were windowed after incubation at 38.5°C for 2 or 3 days. At the appropriate Hamburger and Hamilton (HH) stage of development (Hamburger and Hamilton, 1951), we removed the extra-embryonic membranes to inject plasmids or dsRNA into the central canal of the spinal cord (Wilson and Stoeckli, 2012). All experiments were in accordance with the regulations of the Cantonal Veterinary Office Zurich. We used miR-based constructs encoding GFP as a transfection marker followed by the miR sequence at 250 ng/µl for β-actin-driven constructs or 700 ng/µl for Math1-driven constructs (Wilson and Stoeckli, 2011) (for miR constructs see Table S2). Alternatively, we used a combination of dsRNA (300 ng/µl) and a plasmid encoding GFP (25 ng/µl) in PBS with 0.02% Fast Green (AppliChem). For electroporation, we used the same settings as described previously (Pekarik et al., 2003). Embryos were sacrificed at the desired HH stage and their spinal cords were analyzed as open-book preparations as described (Perrin and Stoeckli, 2000). Injections and electroporations of dsRNA or miR were carried out at HH13-15 (E2) or at HH17/18 (E3). Analyses of commissural axon pathfinding were performed at HH25 (E5), except for the experiment reported in Fig. S1, where the analysis was carried out 1 day later (E6/HH28).

The polymerase II-driven miR constructs were cloned as described previously (Wilson and Stoeckli, 2011). We inserted the miR hairpin-loop structure using *Nhe*I and *Mlu*I (both NEB) to create either β-actin-driven or Math1-driven plasmids (Table S2). We used bp 4283-4995 of the 3′ UTR of chicken calsyntenin 1 (NM_001197050.1) to produce dsRNA (dsCst1) according to our published protocol (Bourikas et al., 2005). For dsCst2 we used bp 498-1436 of chicken calsyntenin 2 (XM_422633.4) and for dsCst3 bp 2175-3169 of chicken calsyntenin 3 (XM_416520.4).

Hypomorphic dosages

To mimic double-heterozygous approaches, which are often used in genetic analyses, we lowered the injected amount of each construct to levels that did not effectively interfere with axon guidance. The co-injection of two miR constructs targeting different genes was expected to interfere with axonal navigation if the two target genes work in the same pathway. The feasibility of this approach has been demonstrated previously in our analyses of the role of Shh in post-crossing commissural axon guidance (Wilson and Stoeckli, 2013). To determine the hypomorphic amounts of the injected miR constructs, we typically used half of the concentration (350 ng/µl) that was used for effective gene silencing. An exception was Math1-miRobo1, where we had to lower the concentration to 300 ng/µl.

Quantification of axon guidance phenotypes

Open-book preparations were imaged using an Olympus BX61 spinning disc microscope. A person blind to the experimental condition scored 10-15 open-book preparations with 11±3 injection sites per treatment group. Only injection sites with GFP expression were included. We distinguished between three phenotypes: normal floor plate crossing and turning rostrally along the contralateral floor plate border; floor plate stalling; and no axonal turns at the contralateral floor plate border. Because it is impossible to count individual axons, we scored an injection site as showing floor plate stalling only when at least 50% of the DiI-labeled axons failed to reach the contralateral floor plate border. Similarly, for the 'no turning' phenotype at least 50% of the axons at the floor plate exit site had to fail to turn rostrally. Obviously, these two phenotypes are not completely independent of each other, as stalling of all axons in the floor plate would prevent the analysis of their turning behavior at the floor plate exit site. Therefore, we only compared the percentages of injection sites per embryo exhibiting normal axon guidance in our quantitative analyses. Statistical analysis of the data was performed with SPSS (IBM). Normal distribution of the values was verified with the Shapiro-Wilk test ($P{\geq}0.01$). P-values were calculated with one-way ANOVA and Tukey's post-hoc tests.

Cultures of commissural neural explants, dissociated dorsal root ganglion neurons and COS7 cells

Explants of commissural neurons were dissected from untreated, control-treated or experimental embryos at HH25. Neurons were plated in 8-well Lab-Tek dishes coated with polylysine (20 μg/ml) and laminin (10 μg/ml). Dorsal root ganglion neurons at a density of 10,000 cells/cm^2 and commissural neurons were cultured for 24-36 h as described previously (Stoeckli et al., 1996, 1997).

To determine surface expression levels, cells were stained with primary antibody against the N-terminal tag before fixation and permeabilization. In all other experiments, cells were fixed and then permeabilized for immunohistochemistry using goat anti-Flag (Abcam), rabbit anti-HA (Rockland) and mouse anti-myc (9E10; Developmental Studies Hybridoma Bank), visualized by goat anti-mouse Cy3 (Jackson ImmunoResearch), donkey anti-rabbit Cy3 (Jackson ImmunoResearch), goat anti-mouse Alexa 488 (Molecular Probes), donkey anti-goat Alexa 488 (Invitrogen) or donkey anti-rabbit Alexa 488 (Jackson ImmunoResearch). For triple staining we also used goat anti-mouse Alexa 350 (Molecular Probes) and goat anti-rabbit Alexa 350 (Invitrogen). Details of antibodies are provided in Table S4. Immunolabeled cells were imaged with a Leica SP2 confocal microscope using a 63× oil-immersion objective (NA=1.4) and an Olympus BX61 spinning disc microscope with a 60× oil-immersion objective (NA=1.42). Image stacks (embracing the Nyquist criterion) were processed using Huygens 3D deconvolution and analysis software. At least 20 cells per condition were included in the quantitative analysis. Neurite length measurements and image analyses were performed with Imaris (Bitplane). Values were analyzed for normal distribution with the Shapiro-Wilk test and *P*-values were calculated with one-way ANOVA and Tamhane's post-hoc tests.

COS7 cells grown in DMEM (Invitrogen) supplemented with 2% fetal calf serum (FCS) were regularly passaged to avoid confluence. For transfection, cells were incubated in 150 μl DMEM with 10% FCS and 50 μl transfection solution containing 250-400 ng DNA (for single transfection) and 1.25% Lipofectamine (Invitrogen) in Opti-MEM (Gibco). For a list of transfected plasmids see Table S3.

In situ hybridization and immunohistochemistry

In situ hybridization was performed as previously described (Mauti et al., 2006). Spinal cord patterning was assessed as previously described (Avilés and Stoeckli, 2016). Commissural axons were stained with a rabbit anti-axonin 1 antibody (Table S4).

Supplementary information
Supplementary information available online at
http://dev.biologists.org/lookup/suppl/doi:10.1242/dev.127449/-/DC1

References
Andermatt, I., Wilson, N. H., Bergmann, T., Mauti, O., Gesemann, M., Sockanathan, S. and Stoeckli, E. T. (2014). Semaphorin 6B acts as a receptor in post-crossing commissural axon guidance. *Development* **141**, 3709-3720.

Augsburger, A., Schuchardt, A., Hoskins, S., Dodd, J. and Butler, S. (1999). BMPs as mediators of roof plate repulsion of commissural neurons. *Neuron* **24**, 127-141.

Avilés, E. C. and Stoeckli, E. T. (2016). Canonical Wnt signaling is required for commissural axon guidance. *Dev. Neurobiol*. **76**, 190-208.

Baudet, M.-L., Zivraj, K. H., Abreu-Goodger, C., Muldal, A., Armisen, J., Blenkiron, C., Goldstein, L. D., Miska, E. A. and Holt, C. E. (2012). miR-124 acts through CoREST to control onset of Sema3A sensitivity in navigating retinal growth cones. *Nat. Neurosci*. **15**, 29-38.

Bourikas, D., Pekarik, V., Baeriswyl, T., Grunditz, Å., Sadhu, R., Nardó, M. and Stoeckli, E. T. (2005). Sonic hedgehog guides commissural axons along the longitudinal axis of the spinal cord. *Nat. Neurosci*. **8**, 297-304.

Brose, K., Bland, K. S., Wang, K. H., Arnott, D., Henzel, W., Goodman, C. S., Tessier-Lavigne, M. and Kidd, T. (1999). Slit proteins bind Robo receptors and have an evolutionarily conserved role in repulsive axon guidance. *Cell* **96**, 795-806.

Charoy, C., Nawabi, H., Reynaud, F., Derrington, E., Bozon, M., Wright, K., Falk, J., Helmbacher, F., Kindbeiter, K. and Castellani, V. (2012). gdnf activates midline repulsion by Semaphorin3B via NCAM during commissural axon guidance. *Neuron* **75**, 1051-1066.

Charron, F., Stein, E., Jeong, J., McMahon, A. P. and Tessier-Lavigne, M. (2003). The morphogen sonic hedgehog is an axonal chemoattractant that collaborates with netrin-1 in midline axon guidance. *Cell* **113**, 11-23.

Chédotal, A. (2011). Further tales of the midline. *Curr. Opin. Neurobiol*. **21**, 68-75.

Chen, Z., Gore, B. B., Long, H., Ma, L. and Tessier-Lavigne, M. (2008). Alternative splicing of the Robo3 axon guidance receptor governs the midline switch from attraction to repulsion. *Neuron* **58**, 325-332.

D'Adamo, P., Menegon, A., Lo Nigro, C., Grasso, M., Gulisano, M., Tamanini, F., Bienvenu, T., Gedeon, A. K., Oostra, B., Wu, S.-K. et al. (1998). Mutations in GDI1 are responsible for X-linked non-specific mental retardation. *Nat. Genet*. **19**, 134-139.

Delloye-Bourgeois, C., Jacquier, A., Charoy, C., Reynaud, F., Nawabi, H., Thoinet, K., Kindbeiter, K., Yoshida, Y., Zagar, Y., Kong, Y. et al. (2015). PlexinA1 is a new Slit receptor and mediates axon guidance function of Slit C-terminal fragments. *Nat. Neurosci*. **18**, 36-45.

Domanitskaya, E., Wacker, A., Mauti, O., Baeriswyl, T., Esteve, P., Bovolenta, P. and Stoeckli, E. T. (2010). Sonic hedgehog guides post-crossing commissural axons both directly and indirectly by regulating Wnt activity. *J. Neurosci*. **30**, 11167-11176.

Hamburger, V. and Hamilton, H. L. (1951). A series of normal stages in the development of the chick embryo. *J. Morphol*. **88**, 49-92.

Hintsch, G., Zurlinden, A., Meskenaite, V., Steuble, M., Fink-Widmer, K., Kinter, J. and Sonderegger, P. (2002). The calsyntenins – a family of postsynaptic membrane proteins with distinct neuronal expression patterns. *Mol. Cell. Neurosci*. **21**, 393-409.

Islam, S. M., Shinmyo, Y., Okafuji, T., Su, Y., Naser, I. B., Ahmed, G., Zhang, S., Chen, S., Ohta, K., Kiyonari, H. et al. (2009). Draxin, a repulsive guidance protein for spinal cord and forebrain commissures. *Science* **323**, 388-393.

Kennedy, T. E., Serafini, T., de La Torre, J. R. and Tessier-Lavigne, M. (1994). Netrins are diffusible chemotropic factors for commissural axons in the embryonic spinal cord. *Cell* **78**, 425-435.

Konecna, A., Frischknecht, R., Kinter, J., Ludwig, A., Steuble, M., Meskenaite, V., Indermühle, M., Engel, M., Cen, C., Mateos, J.-M. et al. (2006). Calsyntenin-1 docks vesicular cargo to kinesin-1. *Mol. Biol. Cell* **17**, 3651-3663.

Lyuksyutova, A. I., Lu, C.-C., Milanesio, N., King, L. A., Guo, N., Wang, Y., Nathans, J., Tessier-Lavigne, M. and Zou, Y. (2003). Anterior-posterior guidance of commissural axons by Wnt-frizzled signaling. *Science* **302**, 1984-1988.

Mauti, O., Sadhu, R., Gemayel, J., Gesemann, M. and Stoeckli, E. T. (2006). Expression patterns of plexins and neuropilins are consistent with cooperative and separate functions during neural development. *BMC Dev. Biol*. **6**, 32.

Nawabi, H. and Castellani, V. (2011). Axonal commissures in the central nervous system: how to cross the midline? *Cell. Mol. Life Sci*. **68**, 2539-2553.

Nawabi, H., Briançon-Marjollet, A., Clark, C., Sanyas, I., Takamatsu, H., Okuno, T., Kumanogoh, A., Bozon, M., Takeshima, K., Yoshida, Y. et al. (2010). A midline switch of receptor processing regulates commissural axon guidance in vertebrates. *Genes Dev*. **24**, 396-410.

Niederkofler, V., Baeriswyl, T., Ott, R. and Stoeckli, E. T. (2010). Nectin-like molecules/SynCAMs are required for post-crossing commissural axon guidance. *Development* **137**, 427-435.

Okada, A., Charron, F., Morin, S., Shin, D. S., Wong, K., Fabre, P. J., Tessier-Lavigne, M. and McConnell, S. K. (2006). Boc is a receptor for sonic hedgehog in the guidance of commissural axons. *Nature* **444**, 369-373.

Onishi, K., Shafer, B., Lo, C., Tissir, F., Goffinet, A. M. and Zou, Y. (2013). Antagonistic functions of Dishevelleds regulate Frizzled3 endocytosis via filopodia tips in Wnt-mediated growth cone guidance. *J. Neurosci*. **33**, 19071-19085.

Parra, L. M. and Zou, Y. (2010). Sonic hedgehog induces response of commissural axons to Semaphorin repulsion during midline crossing. *Nat. Neurosci*. **13**, 29-35.

Pekarik, V., Bourikas, D., Miglino, N., Joset, P., Preiswerk, S. and Stoeckli, E. T. (2003). Screening for gene function in chicken embryo using RNAi and electroporation. *Nat. Biotechnol*. **21**, 93-96.

DEVELOPMENT

Perrin, F. E. and Stoeckli, E. T. (2000). Use of lipophilic dyes in studies of axonal pathfinding in vivo. *Microsc. Res. Technol.* **48**, 25-31.

Pfeffer, S. and Aivazian, D. (2004). Targeting Rab GTPases to distinct membrane compartments. *Nat. Rev. Mol. Cell Biol.* **5**, 886-896.

Philipp, M., Niederkofler, V., Debrunner, M., Alther, T., Kunz, B. and Stoeckli, E. T. (2012). RabGDI controls axonal midline crossing by regulating Robo1 surface expression. *Neural Dev.* **7**, 36.

Ponomareva, O. Y., Holmen, I. C., Sperry, A. J., Eliceiri, K. W. and Halloran, M. C. (2014). Calsyntenin-1 regulates axon branching and endosomal trafficking during sensory neuron development in vivo. *J. Neurosci.* **34**, 9235-9248.

Seabra, M. C., Mules, E. H. and Hume, A. N. (2002). Rab GTPases, intracellular traffic and disease. *Trends Mol. Med.* **8**, 23-30.

Shafer, B., Onishi, K., Lo, C., Colakoglu, G. and Zou, Y. (2011). Vangl2 promotes Wnt/planar cell polarity-like signaling by antagonizing Dvl1-mediated feedback inhibition in growth cone guidance. *Dev. Cell* **20**, 177-191.

Steuble, M., Gerrits, B., Ludwig, A., Mateos, J. M., Diep, T.-M., Tagaya, M., Stephan, A., Schätzle, P., Kunz, B., Streit, P. et al. (2010). Molecular characterization of a trafficking organelle: dissecting the axonal paths of calsyntenin-1 transport vesicles. *Proteomics* **10**, 3775-3788.

Steuble, M., Diep, T.-M., Schätzle, P., Ludwig, A., Tagaya, M., Kunz, B. and Sonderegger, P. (2012). Calsyntenin-1 shelters APP from proteolytic processing during anterograde axonal transport. *Biol. Open* **1**, 761-774.

Stoeckli, E. T. (2006). Longitudinal axon guidance. *Curr. Opin. Neurobiol.* **16**, 35-39.

Stoeckli, E. T. and Landmesser, L. T. (1995). Axonin-1, Nr-CAM, and Ng-CAM play different roles in the in vivo guidance of chick commissural neurons. *Neuron* **14**, 1165-1179.

Stoeckli, E. T., Ziegler, U., Bleiker, A. J., Groscurth, P. and Sonderegger, P. (1996). Clustering and functional cooperation of Ng-CAM and axonin-1 in the substratum-contact area of growth cones. *Dev. Biol.* **177**, 15-29.

Stoeckli, E. T., Sonderegger, P., Pollerberg, G. E. and Landmesser, L. T. (1997). Interference with axonin-1 and NrCAM interactions unmasks a floor-plate activity inhibitory for commissural axons. *Neuron* **18**, 209-221.

Vogt, L., Schrimpf, S. P., Meskenaite, V., Frischknecht, R., Kinter, J., Leone, D. P., Ziegler, U. and Sonderegger, P. (2001). Calsyntenin-1, a proteolytically processed postsynaptic membrane protein with a cytoplasmic calcium-binding domain. *Mol. Cell. Neurosci.* **17**, 151-166.

Wilson, N. H. and Stoeckli, E. T. (2011). Cell type specific, traceable gene silencing for functional gene analysis during vertebrate neural development. *Nucleic Acids Res.* **39**, e133.

Wilson, N. H. and Stoeckli, E. T. (2012). In ovo electroporation of miRNA-based plasmids in the developing neural tube and assessment of phenotypes by dii injection in open-book preparations. *J. Vis. Exp.* pii: 4384.

Wilson, N. H. and Stoeckli, E. T. (2013). Sonic hedgehog regulates its own receptor on postcrossing commissural axons in a glypican1-dependent manner. *Neuron* **79**, 478-491.

Yuan, W., Zhou, L., Chen, J.-H., Wu, J. Y., Rao, Y. and Ornitz, D. M. (1999). The mouse SLIT family: secreted ligands for ROBO expressed in patterns that suggest a role in morphogenesis and axon guidance. *Dev. Biol.* **212**, 290-306.

Zelina, P., Blockus, H., Zagar, Y., Péres, A., Friocourt, F., Wu, Z., Rama, N., Fouquet, C., Hohenester, E., Tessier-Lavigne, M. et al. (2014). Signaling switch of the axon guidance receptor Robo3 during vertebrate evolution. *Neuron* **84**, 1258-1272.

Zou, Y., Stoeckli, E., Chen, H. and Tessier-Lavigne, M. (2000). Squeezing axons out of the gray matter: a role for slit and semaphorin proteins from midline and ventral spinal cord. *Cell* **102**, 363-375.

DEVELOPMENT